Int. J. Multiphase Flow Vol. 17, No. 3, pp. 291–307, 1991
Printed in Great Britain

0301-9322/91 $3.00 + 0.00
Pergamon Press/Elsevier

TWO-PHASE BUBBLY–DROPLET FLOW THROUGH A CONTRACTION: EXPERIMENTS AND A UNIFIED MODEL

B. COUËT,† P. BROWN‡ and A. HUNT
Schlumberger Cambridge Research, High Cross, Madingley Road, Cambridge, England

(Received 16 October 1989; in revised form 24 October 1990)

Abstract—We have derived a consistent and general set of equations to describe the motion of two phases (or components) in flow through a contraction. One phase is continuous, the other dispersed and the range of density ratios ρ is wide. Given the density and flowrate of each component of the flow, the pressure, velocities and void fractions can be computed at any location along the pipe. The single-phase limit as well as the homogeneous-flow limit are both contained within our set of equations. The full mathematical model, based on the so-called interstitial velocity, requires only one fluid-dependent empirical input—the terminal rise (or fall) velocity U_t of a single bubble (or droplet). In the text, the word "bubbles" is to be thought of as the dispersed or discontinuous component of the flow and may refer to air bubbles in water flow, oil drops in oil or water flow or water drops in air or oil flow. Extensive comparisons between results from the model and experimental data obtained in the Schlumberger Cambridge Research multiphase flow loop are presented and show very good agreement in predicting pressure from input flowrates. Our results demonstrate that, although the model is one-dimensional and neglects local bubble–bubble interactions, it is nevertheless robust in dealing with vertical flow and a wide range of density ratios with only one parameter (U_t) necessary for calibration. For two density ratios ρ of 1000 and 1.26, the agreement between the mathematical predictions and the experiments was good in vertical flow. The implication of this conclusion is that the model should perform well at any intermediate values of the density ratio.

Key Words: bubbles, droplets, contraction, multiphase flows

1. INTRODUCTION

Flow systems involving a mixture of gas and liquid or liquid and liquid occur commonly in the petroleum industry. Of particular interest is the prediction of pressure drop for mixtures such as gas bubbles in oil or water, or oil droplets in water flowing through varying geometries. One of the fundamental requirements for equipment design procedures is to formulate correctly a mathematical model for a two-phase flow system with a wide range of density ratios.

The mathematical model described here differs from most of the previous works in that it is a unified model being able to treat air–water as well as oil–water mixtures. It is also based on the so-called interstitial velocity, i.e. the velocity of the unperturbed liquid between the bubbles (or far from the bubble, in the case of one bubble), rather than on the average velocities as is most often done in the segregated or two-fluid models. Drew & Lahey (1979) and Biesheuvel & van Wijngaarden (1984) gave good descriptions of the two-fluid models as essentially a suitable volume average of the conservation equations for each of the two phases, with interaction forces sometimes grafted to it. Most general-purpose models used for engineering applications today are two-fluid models. In recent developments of these models, Lewis & Davidson (1985) and, more recently, Kuo & Wallis (1988) considered the one-dimensional equations of motion for a bubble flowing through a nozzle. But even these models did not allow for the effects on the flowrate of the liquid caused by the presence of flowing bubbles or droplets and, in particular, by the relative velocity (or slip) between the bubbles and the liquid. These effects were considered in a new analysis by Kowe *et al.* (1988), who compared their model with the measurements of Lewis & Davidson (1985). The approach and derivation of the equations of motion reported here follows and extends that given by Kowe *et al.* (1988) and is similar in principle to the mathematical formulation given by Cook & Harlow (1984).

†Schlumberger-Doll Research, Old Quarry Road, Ridgefield, CT 06877-4108.
‡Schlumberger Perforating and Testing, 14910 Airline Road, Rosharon, Tex., U.S.A.

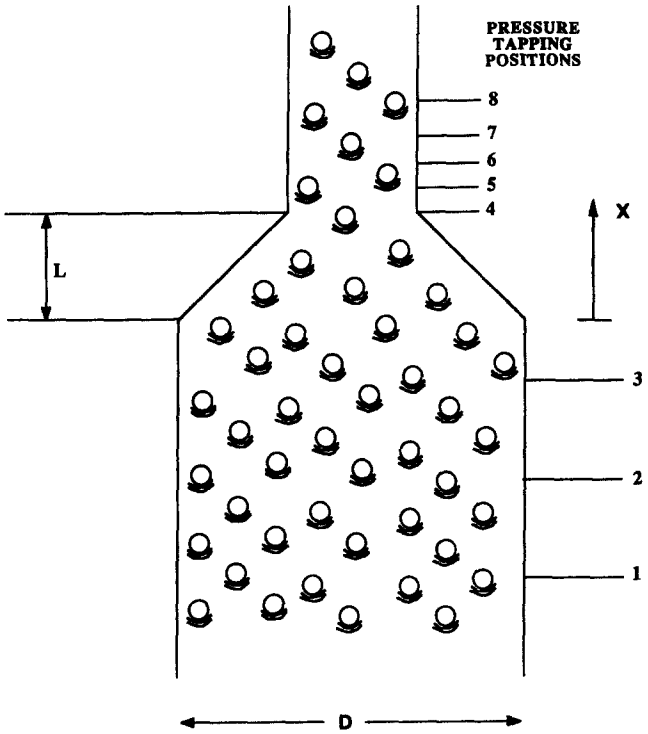

Figure 1. Contraction geometry and pressure tapping locations.

This paper first describes the equations of motion for a bubbly or droplet flow through a pipe with varying internal geometry, more precisely through a vertical contraction (figure 1). When the two phases move at the same velocity the mathematical model reduces to the limit of the flow of an equivalent fluid with the same mixture density. The second part of the paper consists of new experimental results using a multiphase flow loop at Schlumberger Cambridge Research. Velocity and pressure data have been acquired for different flowrates of air bubbles in water or oil droplets in water, both in vertical and inclined flows. Comparisons with the model presented here are restricted to wall pressure measurements for the vertical cases.

2. DEFINITIONS AND ASSUMPTIONS

We consider flow in a vertical pipe of varying cross-sectional area $A(x)$, where the x-axis is streamwise vertically up the pipe. The flow is considered statistically stationary, i.e. there is no time variation in the temporal averages of fluctuating quantities over a time period T. The integral

$$\frac{1}{T}\int_0^T R(x, y, z, t)\,\mathrm{d}t \qquad [1]$$

is therefore constant at any spatial point. $R(x, y, x, t)$ can represent, for example, the pressure, the velocities or the void fractions.

We mention at this point the more important of the numerous assumptions made in the analysis of a bubbly flow, as in Kowe *et al.* (1988). It is assumed that the bubbles are rigid spheres all of the same density ρ_b and volume V_b and with a small diameter compared with the pipe diameter. Note that the word "bubbles" is to be thought of here as the dispersed or discontinuous component of the flow and may refer to air bubbles in water flow or oil drops in water flow. The bubbly flow considered is of a dispersed nature. No explicit account is taken of the effects of liquid- and bubble-density variations, unsteady drag, liquid turbulence generated by mean shear and bubble wakes and the bubble–wall and liquid–wall friction forces. The velocity profiles are flat, akin to a turbulent single-phase pipe flow and although the results are not presented here, local liquid velocity surveys indicate that even at low void fractions this is a good assumption. It is further

assumed that all bubbles at a given cross section move with the same velocity, i.e. the velocity has been averaged so that the description of the flow is one-dimensional.

In this one-dimensional system, all flow variables are taken to be spatial averages over the pipe cross section. The void fraction, for example, normally defined as the ratio of the volume of the light phase over the total volume of both phases, is given by

$$\epsilon_b(x) \equiv \frac{1}{A}\int_A \epsilon_b(x, y, z)\, dA. \qquad [2]$$

The subscript b or B refers to the discontinuous or dispersed phase (bubbles), while the subscript l or L refers to the continuous phase (liquid) so that the liquid void fraction (or liquid holdup) is $\epsilon_l(x)$. It is also understood, but not explicitly stated for the discussion that follows, that in general, all flow parameters are dependent on x.

Some of the nomenclature used in this paper will now be described. If there are n bubbles per unit volume, the void fraction, as introduced above, is simply

$$\epsilon_b = nV_b \qquad [3]$$

and the liquid holdup is just $\epsilon_l = 1 - \epsilon_b$.

Bubbles are assumed to move with a velocity u_b. The bubble-phase superficial velocity u_B is given by

$$u_B \equiv \frac{Q_b}{A}, \qquad [4]$$

where Q_b is the volume flowrate of the discontinuous or dispersed phase. The average bubble velocity is then

$$\langle u_b \rangle \equiv \frac{Q_b}{\epsilon_b A} = \frac{u_B}{\epsilon_b}. \qquad [5]$$

Note here that $\langle u_b \rangle = u_b$ since all bubbles are assumed to move with the same velocity at a given cross section of the flow.

For the liquid, the superficial velocity u_L is given by

$$u_L \equiv \frac{Q_l}{A}, \qquad [6]$$

where Q_l is the liquid volume flowrate. The liquid average velocity is then

$$\langle u_l \rangle \equiv \frac{Q_l}{\epsilon_l A} = \frac{u_L}{\epsilon_l}. \qquad [7]$$

The concept of the interstitial velocity u_l, as introduced above and in Kowe *et al.* (1988), serves to represent the liquid velocity in the space between the bubbles; u_l can be thought of as the background velocity field determining the motion of any bubble in a low void fraction mixture. u_L and thus $\langle u_l \rangle$ can be expressed in terms of the interstitial velocity by introducing the concept of virtual mass in the displacement of the bubbles through the liquid. When a body moves uniformly through an infinite volume of incompressible inviscid fluid at rest, it induces a drift in the fluid such that the drift-volume of fluid is equal to $C_m V$, where V is the volume of the body and C_m is known as the added-mass coefficient (Darwin 1953). For a rigid sphere C_m has the value 0.5 (Lamb 1945). For the present formulation, bubbles are modelled as rigid spheres and so the virtual mass concept must also be introduced as in Kowe *et al.* (1988). Then the liquid flowrate across a surface area A is

$$Q_l = u_L A = [(1 - \epsilon_b)u_l + \epsilon_b C_m(u_b - u_l)]A, \qquad [8]$$

wherein use has been made of the relation $\epsilon_l = 1 - \epsilon_b$, and $u_b - u_l$ is known as the relative velocity. Combining [7] and [8], the liquid average velocity can now be rewritten as

$$\langle u_l \rangle = u_l + \frac{\epsilon_b}{\epsilon_l} C_m(u_b - u_l). \qquad [9]$$

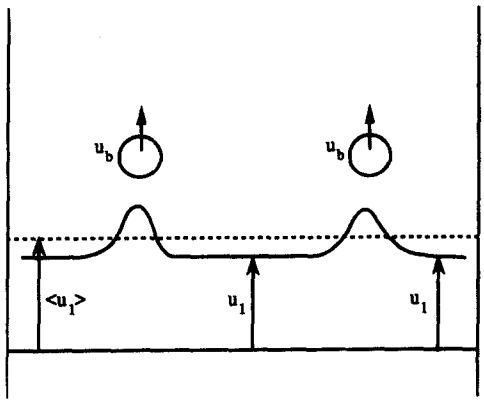

Figure 2. Illustration showing the bubble velocity u_b, the interstitial velocity u_l and the liquid average velocity $\langle u_l \rangle$.

Figure 2, similar to figure 1 in Kowe *et al.* (1988), illustrates how the distinction between interstitial and average velocity is associated with the liquid transported by the bubbles.

The interstitial velocity can also be rewritten in terms of the volume flowrates and the bubble velocity, making use of [4]–[9]:

$$u_l = \frac{(Q_l - C_m Q_b)u_b}{Au_b - (1 + C_m)Q_b}. \quad [10]$$

The above expression will be used later in the solution procedure.

3. EQUATIONS OF MOTION

3.1. Equations of mass conservation

With the definition of void fraction given in the previous section, a simple conservation relationship relates the two components of the flow:

$$\epsilon_b + \epsilon_l = 1. \quad [11]$$

Each component of the flow also obeys its own mass-conservation law stating that the flowrate, once specified at the inlet, is constant throughout the pipe for steady flow and constant densities, i.e.

$$\frac{d}{dx}(A\epsilon_b\langle u_b \rangle) = 0 \quad [12]$$

and

$$\frac{d}{dx}(A\epsilon_l\langle u_l \rangle) = 0. \quad [13]$$

3.2. Momentum equation for bubbles in liquid flow

The momentum equation for a single bubble in an unsteady liquid flow can be written in terms of a generalized force equation as follows (Thomas *et al.* 1983):

$$\rho_b V_b \frac{D_b u_b}{Dt} = F_b, \quad [14]$$

where F_b is the resultant force acting on a rigid spherical bubble of volume V_b moving at a velocity u_b. The material derivative is defined as

$$\frac{D_b}{Dt} \equiv \frac{\partial}{\partial t} + u_b \frac{\partial}{\partial x}. \quad [15]$$

If there are n bubbles per unit volume and use is made of [3], the momentum equation for the dispersed phase is then

$$\epsilon_b \rho_b \frac{D_b u_b}{Dt} = nF_b. \qquad [16]$$

Thomas *et al.* (1983) first considered the inviscid flow around a spherical bubble. This is an appropriate model when the bubble Reynolds number (defined in terms of the bubble diameter and relative velocity) is large [>1000, equivalent to a diameter of 5 mm and a rise velocity in water of 15–25 cm/s (Clift *et al.* 1978)] and the water is pure. If the bubbles are also sufficiently small that there is local homogeneity in the flow velocity gradients, the bubble velocity will depend only on the interstitial liquid velocity and its first derivatives. With this assumption of local homogeneity, Thomas *et al.* (1983) have then assumed that drag can be added to the force derived for inviscid flow and, for a sufficiently low void fraction, that bubble–bubble interactions can also be neglected. F_b can thus be decomposed into four uncoupled contributions,

$$F_b = F_p + F_g + F_v + F_d, \qquad [17]$$

which are now described.

If the x-axis is streamwise and upwards, the force F_p due to the pressure gradient in the liquid far from the bubble is given by

$$F_p = -V_b \frac{\partial p_l}{\partial x} \qquad [18]$$

$$= \rho_l V_b \left(\frac{D_l u_l}{Dt} + g \right), \qquad [19]$$

where p_l is the undisturbed liquid pressure, g is the gravitational acceleration and

$$\frac{D_l}{Dt} \equiv \frac{\partial}{\partial t} + u_l \frac{\partial}{\partial x}. \qquad [20]$$

The gravitational force F_g exerted on the bubble in the absence of the liquid is simply

$$F_g = -\rho_b V_b g, \qquad [21]$$

$|F_g|$ being the weight of the bubble. It may be noted that in the absence of flow, F_p and F_g are frequently combined into what is commonly called the buoyancy force.

The virtual-mass force F_v can be thought of as a drag force in its inviscid limit, i.e. the inertia force due to the local acceleration of the added mass of liquid travelling with the bubble, and is written as

$$F_v = -\left(\frac{D_b I}{Dt} + I \frac{\partial u_l}{\partial x} \right), \qquad [22]$$

where I is the "impulse" of the motion of the bubble [in the sense of Kelvin (Lamb 1945)], i.e. the momentum of the added mass of liquid which travels with the bubble due to the pressure field associated with the motion of the bubble (Thomas *et al.* 1983; Auton *et al.* 1988). I is proportional to the relative velocity, the constant of proportionality as mentioned earlier being the added-mass coefficient C_m:

$$I = \rho_l V_b C_m (u_b - u_l). \qquad [23]$$

Substituting [23] in [22] yields

$$F_v = -\rho_l V_b C_m \left[\frac{\partial}{\partial t}(u_b - u_l) + u_b \frac{\partial}{\partial x}(u_b - u_l) + (u_b - u_l) \frac{\partial u_l}{\partial x} \right]$$

$$= -\rho_l V_b C_m \left(\frac{D_b u_b}{Dt} - \frac{D_l u_l}{Dt} \right). \qquad [24]$$

Recently, Drew & Lahey (1987) have also concluded that this is the correct form for the virtual-mass force, rather than the form suggested in their earlier publications.

The actual drag force F_d on the bubble is due to the viscous stresses changing the pressure distribution around the bubble. Neglecting the non-uniformity and unsteadiness of the surrounding flow, F_d can be expressed in the usual dimensional scaling form as

$$F_d = -\tfrac{1}{2}\rho_l(u_b - u_l)|u_b - u_l| C_d \pi a^2, \qquad [25]$$

where a is the bubble radius and C_d is the drag coefficient. Note that, in our treatment of real bubbles at high Reynolds number, form drag predominates and C_d, normally a function of Reynolds number, is approximately constant (Thomas *et al.* 1983). Therefore, as an alternative, and sometimes more convenient formulation, particularly when the bubble radius and the drag coefficient are unknown, the drag force can be rewritten in terms of U_t, the terminal rise (or fall) velocity of a bubble in an infinite stationary liquid, corresponding to a balance of the gravitational and drag forces (Wallis 1969):

$$U_t^2 = \frac{8|\Delta\rho|ag}{3\rho_l C_d}, \qquad [26]$$

where $\Delta\rho = \rho_b - \rho_l$. This formula leads to

$$F_d = -|\Delta\rho| V_b g \frac{(u_b - u_l)|u_b - u_l|}{U_t^2}. \qquad [27]$$

Although the formulation in terms of U_t is used generally from now on, it should be borne in mind that it rests on the assumption that C_d is independent of the bubble Reynolds number.

Combining the above results leads to the expression for the total force acting on a bubble:

$$F_b = \rho_l V_b \left[\frac{D_l u_l}{Dt} + g - C_m\left(\frac{D_b u_b}{Dt} - \frac{D_l u_l}{Dt}\right) - \frac{\rho_b}{\rho_l} g - g\frac{\Delta\rho|(u_b - u_l)|u_b - u_l|}{\rho_l U_t^2}\right]$$

$$= \rho_l V_b \left[(1 + C_m)\frac{D_l u_l}{Dt} - C_m \frac{D_b u_b}{Dt} - \frac{\Delta\rho}{\rho_l} g - g\frac{|\Delta\rho|(u_b - u_l)|u_b - u_l|}{\rho_l U_t^2}\right]. \qquad [28]$$

In the limit $\rho_b \ll \rho_l$ (i.e. for a gas–liquid system) and for steady flow, the one-dimensional momentum equation for a bubble reduces to $F_b \cong 0$ or

$$C_m u_b \frac{du_b}{dx} \cong (1 + C_m) u_l \frac{du_l}{dx} + g - g\frac{(u_b - u_l)|u_b - u_l|}{U_t^2}, \qquad [29]$$

which is precisely [28] in Kowe *et al.* (1988).

The expression for the total force F_b can also be rewritten explicitly retaining the interstitial pressure gradient [18], which leads to

$$F_b = V_b\left[-\frac{\partial p_l}{\partial x} - \rho_l C_m\left(\frac{D_b u_b}{Dt} - \frac{D_l u_l}{Dt}\right) - \rho_b g - g|\Delta\rho|\frac{(u_b - u_l)|u_b - u_l|}{U_t^2}\right]. \qquad [30]$$

Again assuming steady flow and using [3], the momentum equation for the dispersed phase becomes

$$(\rho_b + \rho_l C_m) u_b \frac{du_b}{dx} - \rho_l C_m u_l \frac{du_l}{dx} = -\frac{dp_l}{dx} - \rho_b g - g|\Delta\rho|\frac{(u_b - u_l)|u_b - u_l|}{U_t^2}. \qquad [31]$$

As for the liquid average pressure $\langle p \rangle$, it may be defined, following Kowe *et al.* (1988) by integrating over the inviscid flow near a bubble. Knowing that the liquid velocity is greater near the bubbles than the interstitial velocity, the difference between the average and the interstitial pressure is seen as being proportional to the square of the relative velocity and to the relative

volume of liquid occupied by the bubbles. $\langle p \rangle$ can be written in terms of the interstitial pressure, p_l, i.e. the liquid pressure between the bubbles on a surface across the flow, as

$$\langle p \rangle = p_l - \frac{\rho_l C_m \epsilon_b (u_b - u_l)^2}{2\epsilon_l}. \quad [32]$$

Equation [32] together with [9] clearly illustrated the difference in going from an average-variable formulation to [31] by introducing extra terms of order ϵ_b. Note that [32] is imbedded in [8.7] and [8.8] of Biesheuvel & van Wijngaarden (1984).

It becomes apparent that [31] is identical to an average-variable equation in the cases when $\epsilon_b \to 0$ or when the relative velocity $u_b - u_l$ is zero. The first case is the single-phase limit, while the second case of no slip between the two components of the flow (homogeneous-flow limit) reduces both equations to an equation similar to Bernoulli's equation where the pressure drop is balanced by the gravitational and the acceleration terms.

3.3. Momentum equation for the liquid component

The momentum-balance equation for the liquid component can be derived mathematically by integrating the unsteady Navier–Stokes equations over a fixed control volume of fluid containing and possibly intersecting bubbles. A thorough mathematical derivation and validation was presented in Kowe *et al.* (1988). Rather than duplicating this previous work here, let us describe the final result as an equation similar to that for the dispersed phase, where the rate of change of liquid momentum is equal to the sum of various forces acting on the control volume. The momentum-balance equation can then be physically explained in terms of these different force contributions.

On one side of the steady-state momentum-balance equation is the variation of the liquid momentum flux given by

$$\frac{\mathrm{d}}{\mathrm{d}x}\left[\rho_l A u_l^2 + \frac{2\epsilon_b}{5\epsilon_l} A \rho_l C_m (u_b - u_l)^2\right],$$

where the first term is the momentum flux in the absence of bubbles, i.e. in the unperturbed fluid far away from the bubbles (the change of liquid momentum flux due the presence of bubbles within the control surface will be incorporated later). The second term is the additional momentum flux in the liquid at the surface of the control volume and caused by the flow near the spherical bubbles as in Kowe *et al.* (1988). On the other side of the equation are the pressure forces arising from the boundaries of the control volume, the weight of the liquid and the force due to the presence of bubbles in the control volume.

The streamwise pressure force acting across the control volume is simply $-\mathrm{d}(A\langle p \rangle)/\mathrm{d}x$. The pressure force per unit length on the walls can in turn be written as $p_w \, \mathrm{d}A/\mathrm{d}x$, where p_w is the wall pressure, i.e. the pressure that would be measured by a transducer on the wall. With a one-dimensional flow approximation and since wall friction forces are neglected, it is *assumed* that the wall pressure is the same as the average liquid pressure $\langle p \rangle$ across the flow.

The weight per unit length of the liquid is given simply by $-A\epsilon_l \rho_l g$.

Following the derivation in section 3.2 of the resultant force F_b acting on a bubble, it should be noted that some components of F_b are forces due to the liquid motion, i.e. they are interfacial forces acting on the bubble. In fact, $F_b - F_g$ is precisely the interfacial force acting on a bubble. Consequently, the reactive component of this force should appear in the liquid momentum equation to take into account the presence of bubbles. Finally, as mentioned earlier, the presence of the bubbles within the control surface also implies a change of momentum of the liquid accelerating with the bubbles (Kowe *et al.* 1988). With the number of bubbles being expressed by ϵ_b and for a steady state, the reactive force per unit pipe length from the bubbles is:

$$-A\epsilon_b\left(\frac{F_b}{V_b} + \rho_b g - \rho_l u_b \frac{\mathrm{d}u_l}{\mathrm{d}x}\right).$$

The last two terms in the above expression are, respectively, the weight of the bubbles and the change of momentum of the liquid accelerating with the bubbles.

Combining all the above force contributions for a steady flow and using [30] yields the liquid momentum equation:

$$\frac{\mathrm{d}}{\mathrm{d}x}\left[\rho_l A u_l^2 + \frac{2\epsilon_b}{5\epsilon_l} A \rho_l C_m (u_b - u_l)^2\right] - \langle p \rangle \frac{\mathrm{d}A}{\mathrm{d}x} + \frac{\mathrm{d}}{\mathrm{d}x}(A\langle p \rangle) - A\epsilon_b \rho_l u_b \frac{\mathrm{d}u_l}{\mathrm{d}x}$$

$$= -A\epsilon_l \rho_l g + A\epsilon_b \left[\frac{\mathrm{d}p_l}{\mathrm{d}x} + \rho_l C_m \left(u_b \frac{\mathrm{d}u_b}{\mathrm{d}x} - u_l \frac{\mathrm{d}u_l}{\mathrm{d}x}\right) + g\,|\Delta\rho|\,\frac{(u_b - u_l)\,|u_b - u_l|}{U_t^2}\right]. \quad [33]$$

Replacing $\langle p \rangle$ in terms of p_l by the use of [32], the l.h.s. of [33] becomes

$$A\frac{\mathrm{d}p_l}{\mathrm{d}x} + 2A\rho_l u_l \frac{\mathrm{d}u_l}{\mathrm{d}x} + \rho_l u_l^2 \frac{\mathrm{d}A}{\mathrm{d}x} - A\epsilon_b \rho_l u_b \frac{\mathrm{d}u_l}{\mathrm{d}x} + H, \quad [34]$$

where

$$H = \frac{\rho_l C_m}{10}\left\{4(u_b - u_l)^2 \frac{\epsilon_b}{\epsilon_l}\frac{\mathrm{d}A}{\mathrm{d}x} - A\frac{\mathrm{d}}{\mathrm{d}x}\left[(u_b - u_l)^2 \frac{\epsilon_b}{\epsilon_l}\right]\right\}. \quad [35]$$

Replacing the l.h.s. of [33] by [34], dividing by A and rearranging the terms yields:

$$\rho_l(2u_l - \epsilon_b u_b)\frac{\mathrm{d}u_l}{\mathrm{d}x} + \rho_l u_l^2 \frac{1}{A}\frac{\mathrm{d}A}{\mathrm{d}x} - \epsilon_b \rho_l C_m \left(u_b \frac{\mathrm{d}u_b}{\mathrm{d}x} - u_l \frac{\mathrm{d}u_l}{\mathrm{d}x}\right) + H$$

$$= -\epsilon_l \frac{\mathrm{d}p_l}{\mathrm{d}x} - \epsilon_l \rho_l g + \epsilon_b g |\Delta\rho| \frac{(u_b - u_l)\,|u_b - u_l|}{U_t^2} \quad [36]$$

for the liquid momentum equation with

$$H = \frac{\rho_l C_m}{10}\left\{4(u_b - u_l)^2 \frac{\epsilon_b}{\epsilon_l}\frac{1}{A}\frac{\mathrm{d}A}{\mathrm{d}x} - \frac{\mathrm{d}}{\mathrm{d}x}\left[(u_b - u_l)^2 \frac{\epsilon_b}{\epsilon_l}\right]\right\}. \quad [37]$$

Here also, as for the bubble momentum equation in the previous section, it is easy to see that [36] reduces to Bernoulli's equation when the relative velocity vanishes (homogeneous-flow limit) as well as for the single-phase flow limit ($\epsilon_b = 0$) (see the appendix).

To arrive at a two-component pressure equation, [31] and [36] are combined by eliminating the drag term between the two equations. This leads to:

$$\frac{\mathrm{d}p_l}{\mathrm{d}x} + (\epsilon_l \rho_l + \epsilon_b \rho_b) g = -\rho_l(2u_l - \epsilon_b u_b)\frac{\mathrm{d}u_l}{\mathrm{d}x} - \rho_l u_l^2 \frac{1}{A}\frac{\mathrm{d}A}{\mathrm{d}x} - \epsilon_b \rho_b u_b \frac{\mathrm{d}u_b}{\mathrm{d}x} - H. \quad [38]$$

Similarly, a velocity equation can be derived by eliminating the pressure gradient between [31] and [36]:

$$\rho_l(2u_l - \epsilon_b u_b)\frac{\mathrm{d}u_l}{\mathrm{d}x} + \rho_l u_l^2 \frac{1}{A}\frac{\mathrm{d}A}{\mathrm{d}x} - \epsilon_l \rho_b u_b \frac{\mathrm{d}u_b}{\mathrm{d}x} - \rho_l C_m \left(u_b \frac{\mathrm{d}u_b}{\mathrm{d}x} - u_l \frac{\mathrm{d}u_l}{\mathrm{d}x}\right) + H$$

$$= g\,\Delta\rho\left[\epsilon_l + \frac{|\Delta\rho|}{\Delta\rho}\frac{(u_b - u_l)\,|u_b - u_l|}{U_t^2}\right]. \quad [39]$$

It is worth noting that [38] reduces to the single-phase Bernoulli equation for $\epsilon_b = 0$. Equation [38] also collapses to a "two-phase Bernoulli equation" when $u_b = u_l$, with ρ_l being replaced by the mixture density $\rho_m \equiv \epsilon_b \rho_b + \epsilon_l \rho_l$.

By a suitable choice of non-dimensional variables, the above set of equations can be transformed into a non-dimensional set such that all the quantities are of order unity. For that purpose, the contraction length L is chosen as the normalizing length and $(Q_l + Q_b)/L^2$ as the normalizing velocity, whereas $Q = Q_b/(Q_l + Q_b)$ defines a non-dimensional flowrate.

4. SOLUTION PROCEDURE

The non-dimensionalized equations are solved in terms of p_l and u_b. What is given is the geometry of the pipe, i.e. $A(x)$, the density of each component of the flow, the terminal rise (or fall) velocity of the bubbles in stationary liquid, U_t, and the constants C_m and g. The equations were solved for pipe length of $7L$, $3L$ ahead of and $3L$ past the contraction. The experiments were run with air bubbles or oil droplets in a water continuous phase. The respective densities are 1, 790 and 1000 kg/m^3. The terminal rise velocity of an air bubble is taken to be 0.25 m/s, whereas the terminal rise velocity of an oil droplet is taken to be 0.15 m/s. These values of terminal velocities are the ones given by the Harmathy relationship (Harmathy 1960):

$$U_t = 1.53\left(\frac{\sigma g(\rho_l - \rho_b)}{\rho_l^2}\right)^{1/4}, \qquad [40]$$

where σ is the interfacial tension. This relationship has been shown to be widely applicable in terms of density differences of flows at low void fraction (Nicolas & Witterholt 1972).

Two boundary conditions are needed at the upstream inlet to solve the two first-order ordinary differential equations and these are taken as the flowrate of the two components of the flow. Knowing the two flowrates, it is sufficient to set p_l and u_b to arbitrary values at the inlet: for a long enough inlet, these two variables will relax to the proper steady value associated with the given flowrates. In the case of the pressure, it can be chosen without loss of generality to be $p_l = 0$ since what is of interest is the pressure variation rather than the absolute pressure through the contraction.

The inlet bubble velocity (as well as u_l and ϵ_b at the inlet) could be readily obtained by solving iteratively, for the case of a fully developed flow, the three non-linear equations [5], [8] and [39]. However, for the sake of computational simplicity and efficiency, its value is obtained by first solving the ordinary differential equations in a straight pipe (with no contraction) of $7L$ to allow the velocity to relax to its constant value appropriate to the given flowrate. For that purpose, the boundary condition at the inlet is set to be

$$u_b = C_0(u_L + u_B) - \frac{|\Delta\rho|}{\Delta\rho} U_t. \qquad [41]$$

C_0 is regarded in the literature (Govier & Aziz 1982) as a distribution coefficient related to the liquid velocity profile and the bubble concentration profile although, in general, there seems to be no physical reason why the same constant should be multiplying both the liquid and bubble velocities. Here C_0 is taken to be a relaxation parameter such that u_b is constant at the inlet of the pipe. The velocity thus obtained is then used to initialize the solution of the differential equations through the contraction.

The profiles of pressure, the velocity of each component and the void fraction of each component can now be determined at all locations along the length of the pipe and through the contraction. For comparison with the experimental data, the pressure drops along the straight section of the pipe and across the contraction will also be obtained.

It may be of value to remind the reader that the approximations inherent to the model are many. The fact that the equations of motion are derived correctly only for low bubbly-phase void fraction (volumetric fraction of bubbles) will be illustrated below in the comparisons with experimental data when the model is used to predict pressure drops at relatively high void fractions. The use of the terminal rise (or drop) velocity of a *single* bubble or droplet in a stationary liquid in the formulation of the drag force on the bubbles or droplets is also an obvious source of discrepancies since it is well-known that as the void fraction increases, the rise (or drop) velocity may change due to mutual interaction. This is particularly evident in the case of gas bubbles which coalesce as the void fraction increases, giving larger faster-moving bubbles, whereas oil droplets tend to behave more like independent solid spheres for the whole range of void fraction considered. Another approximation of seemingly less importance is the fact that the model is one-dimensional and thus assumes that at a given cross section the bubbles or droplets all travel at the same speed, even through the contraction region. The model also considers the flow as being in a steady state which, in itself, constitutes an averaging of the motions.

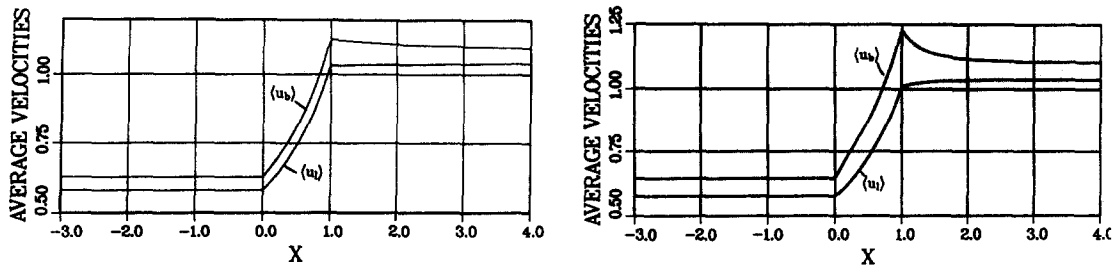

Figure 3. Bubble average velocity $\langle u_b \rangle$ (upper curve) and liquid average velocity $\langle u_l \rangle$ (lower curve) vs the streamwise coordinate x. The left plot is for an oil–water system (density ratio $\rho = 1.266$, $Q = 0.21$) while the right plot is for an air–water system (density ratio $\rho = 1000$, $Q = 0.24$).

5. TYPICAL RESULTS

The aim of this section is to exemplify the results which the one-dimensional model described here is capable of giving. Detailed comparisons with experimental data are documented in a section below.

Figure 3 shows the average velocity profiles for the liquid (lower curve) and for the bubble component (upper curve) of a vertical flow passing through the contraction geometry. The left plot is for an oil–water system while the right one is for an air–water system. Comparing the two plots, it is seen that the air bubbles are subject to a greater acceleration through the contraction section then the oil drops due to their lower density.

Figure 4 shows in the left plot a typical average liquid pressure profile through the contraction. In the straight section, only the hydrostatic contribution is present followed by a pressure drop through the contraction before reverting to a straight hydrostatic profile in the narrower section above the contraction. An interesting phenomenon illustrated by our model in the right plot of figure 4 is the fact that the light-phase void fraction can either increase or decrease through the contraction. The two curves are for two different sets of flowrates, both for the light and the heavy components of the flow.

6. EXPERIMENTAL APPARATUS

The experiments described in this paper were performed in a multiphase flow loop (shown schematically in figure 5) in the Fluid Mechanics Department at Schlumberger Cambridge Research. The working section is made up of 3″ (76.2 mm) nominal bore clear acrylic plastic pipe. Visually it was observed that in both oil–water and air–water conditions the flows were generally made up of bubbles in a diameter range from 3 to 8 mm, though at high void fractions (over about 15%) cap-shaped air bubbles of larger diameter appeared in the air–water flow. The air bubbles tended to form a high concentration rapidly-moving stream at the centre of the pipe, whereas the oil droplets tended to be more evenly distributed. This range of droplet sizes gives a ratio of pipe size to bubble size of between 10 and 25.

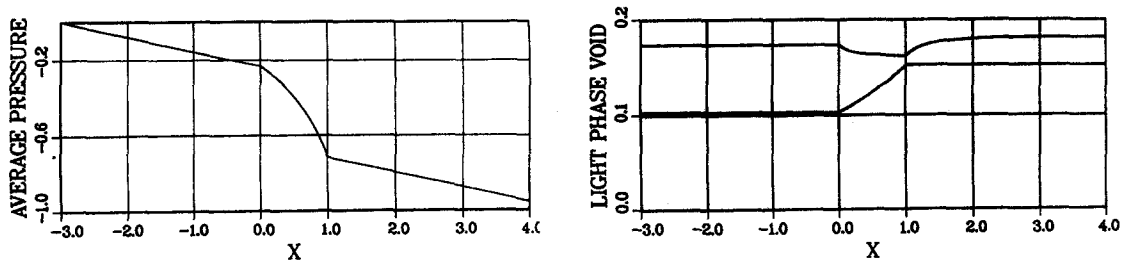

Figure 4. *Left plot*: liquid average pressure $\langle p_l \rangle$ vs the streamwise coordinate x for an oil–water system (density ratio $\rho = 1.266$, $Q = 0.21$). *Right plot*: bubble void fraction ϵ_b vs the streamwise coordinate x for an air–water system (density ratio $\rho = 1000$). The left curve is for $Q = 0.19$ while the bottom curve is for $Q = 0.30$.

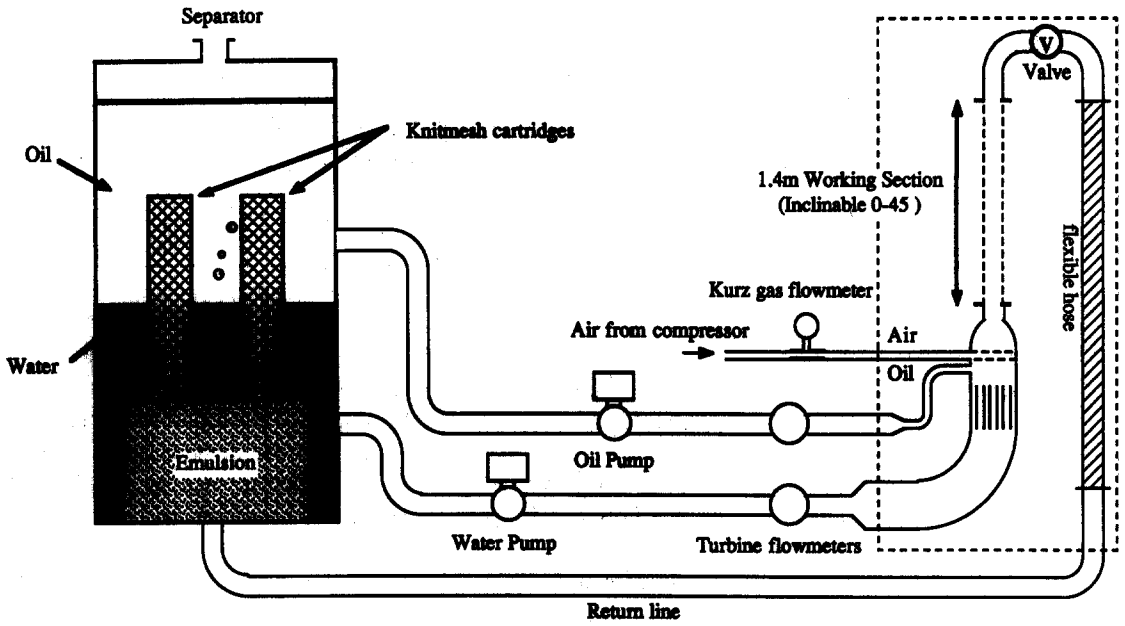

Figure 5. The Schlumberger Cambridge Research multiphase flow loop.

6.1. Air–water flows

For an air–water flow, the water phase is provided from a reservoir tank via a centrifugal pump and the flowrate is measured by one of two turbine meters according to the range required. Air is supplied from a centrifugal compressor via a regulator and control valve to an injection plate which resembles a perforated cartwheel. The air flowrate is measured by a single Kurz Series 505 linear mass flowmeter with a 0–5 V output. This is an industrial grade device with a claimed accuracy of better than 2% of the indicated flowrate (1% at full scale). The output is true mass flowrate at standard conditions, thus obviating the need for local pressure and temperature measurements at the meter.

Having passed through the test section the air–water mixture is returned to the reservoir tank. The geometry of the return line is such that the presence of air does not produce destabilizing back pressures on the system.

6.2. Oil–water flows

The flow loop has the capability of circulating two liquid phases, one phase through the pump and turbine meter arrangement described above, the other through an identical parallel arrangement of pump and turbine meters (with the same technical specifications) before being injected into the primary flow immediately upstream of the working section. To ensure a uniform injection the secondary phase is injected through eight ports equally spaced around the flow.

Once mixed in the test section the two liquids have to be separated before they can be reused. This is achieved by means of the separator illustrated in figure 5. The mixture enters a chamber at the bottom of the separator and thence through an array of six Knitmesh cylinders. Knitmesh is a commercial product consisting of a matrix of two metals with different surface tension properties such that the continuous phase is able to pass straight through, but any small bubbles of the secondary phase are temporarily trapped in the matrix. As the small bubbles accumulate they also agglomerate, until they are of sufficient size that they are either buoyant enough or heavy enough (as the case may be) to be able to separate from the other phase under gravity. With the lighter phase now above the heavier phase, outlets at the top and bottom of the separator tank feed to the appropriate pump for recirculation. Valves are provided for selecting the mode of operation, selecting which turbine meters are to be used, and for choking the flow to facilitate low flowrates when necessary.

The oil used in the experiments described in this paper was an odourless kerosene, with a density of 790 kg/m^3 at 15°C and an absolute viscosity of 1.6 cP at 25°C (manufacturer's figures).

Table 1. Pressure tapping locations

Tapping No.	Axial location (x/L)
1	−12.55
2	−6.86
3	−1.18
4	1.04
5	1.21
6	1.41
7	1.76
8	2.74

Table 2. Axial location of the traverse positions

Traverse location	Axial position (x/L)
A	−6.86
B	−3.13
C	0.39
D	0.98

6.3. *Instrumentation*

The experimental apparatus was designed with a view to maximum automation, and both control functions and data acquisition are supervised by computer. Both pumps are equipped with variable speed controllers which can be controlled by a 0–10 V signal from a remote device. Likewise the air control valve, which operates on a 3–15 psi pressure signal, is controlled in turn by a 4–20 mA signal from the remote device. Hence the flow conditions can be selected and set up by software control.

Two differential pressure transducers were used to monitor the pressure along the pipe at a number of locations, given in table 1 and indicated schematically in figure 1. The position of the tappings is referred to the start of the contraction, and normalized on the length of the contraction, so that the change in flowing area occurs between $x/L = 0$ and $x/L = 1.0$. An arrangement of solenoid valves controlled by the computer allowed the pressure lines to be switched, and also provided the means by which the transducers could be zeroed and the pressure lines regularly flushed through to remove any air or oil present. Both transducers had an effective output of 4–40 mA (4–20 mA nominal) monitored by two digital ammeters.

Control and data acquisition were effected with a BBC microcomputer via an IEEE interface. A 32016 (1 Mbyte) co-processor was used to increase computing speed and memory capacity. Data was stored on floppy disc.

Used in conjunction with the BBC was an autonomous data acquisition and analogue control system (ADU). This device scans up to 16 analogue channels and 4 digital channels simultaneously and either stores the data in its own memory, or communicates directly with the BBC via the IEEE link. Also provided are 4 analogue control outputs supplying 0–10 V, which were used to control the pump speeds and air control valve.

Air flowrate, test section static pressure and test section temperature from a thermocouple were all monitored by the ADU. The output from the water and oil flowmeters were monitored by the BBC via a frequency counter and the differential pressure transducer outputs (4–40 mA) were read by two digital ammeters, all over the IEEE link.

In addition to the pressure tappings, the working section was equiped with a single-axis traverse that could be mounted at various axial locations, as detailed in table 2. A cylindrical hot-film probe could then be traversed across a diameter of the pipe by a stepper motor controlled from the BBC to measure the local void fraction distribution. The method used to interpret the hot-film signal was the PDF and thresholding technique described by Brunn & Farrar (1988).

7. COMPARISONS OF THE EXPERIMENT AND MODEL

The results obtained experimentally were in two parts, firstly the pressure drops across the contraction for an air–water mixture or an oil–water mixture, each for a range of flowrates and secondly more detailed pressure measurements along the pipe. For the pressure drop "across the contraction" we refer to the pressure difference between tappings 3 and 7, a distance of three times the contraction length, and for the more detailed measurements the pressure points marked on figures 7–9 are from tappings 3–8.

The first set of data have been plotted relative to the bubble void fraction just before the flow enters the contraction (actually at pressure tapping 3). Figure 6 shows the percentage difference for the model predictions relative to the experimental pressure drops across the contraction vs

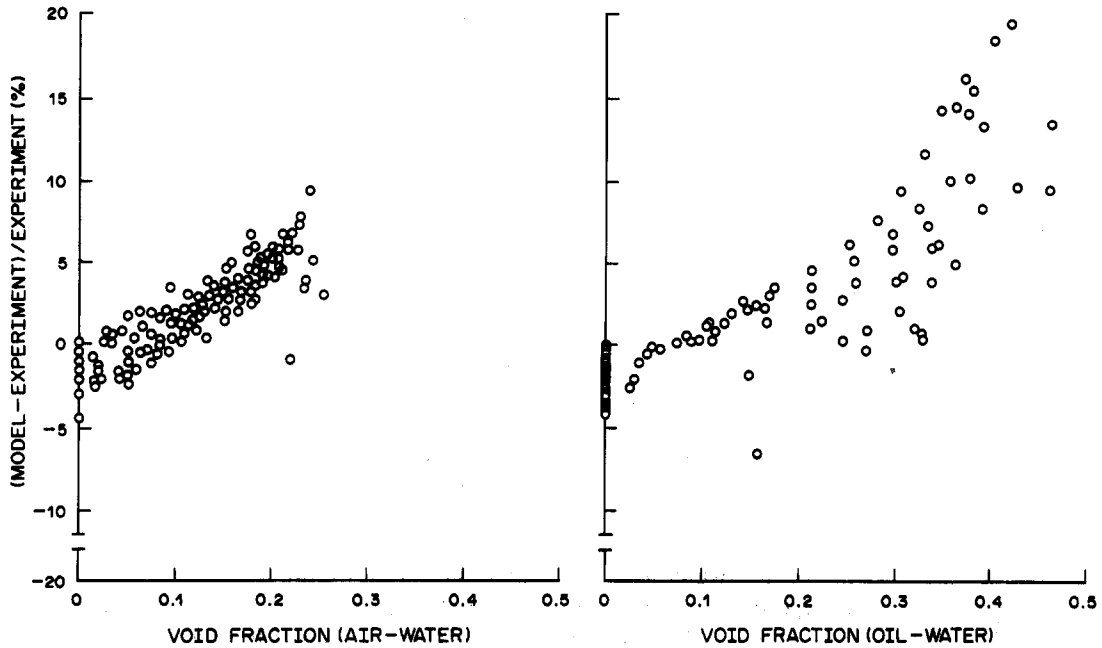

Figure 6. Percentage difference for the model predictions relative to the experimental pressure drops across the contraction vs bubble void fraction for air–water cases on the left and for oil–water cases on the right.

bubble void fraction; the left graph is for the air–water cases and the right one for the oil–water cases. It is clear that the model is accurate to better than 10% up to 30% bubble void fraction. In the dilute region (< 10%) the agreement in both cases is excellent. Since the model assumes no bubble–bubble interactions other than those caused by the change in interstitial velocity, it is not surprising that above 20% bubble void fraction there is an increasing discrepancy between model and experiment. The variation seems to be quadratic, consistent with the limitations of the model. Note also that the accuracy within 5% for the single-phase cases quantifies essentially the variability in the experimental data relative to Bernoulli's equation for loss-free flows. It is also apparent that the experimentally derived single-phase discharge coefficient of 0.984 (i.e. an underestimate of 1.6%) is consistent with the zero void fraction limit of the two-phase results.

Pressure profiles along the pipe as predicted from the model are shown in figures 7 and 8. On each graph the associated experimental points are also shown. In general it can be seen that the

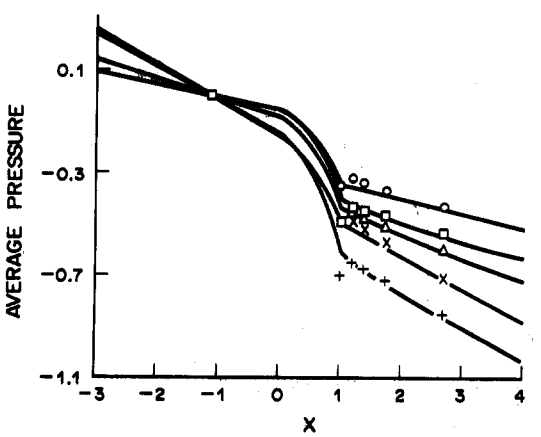

Figure 7. Liquid pressure vs the streamwise coordinate x for air–water cases. +, $Q = 0.13$; □, $Q = 0.22$; △, $Q = 0.29$; ○, $Q = 0.40$; ×, $Q = 0.49$

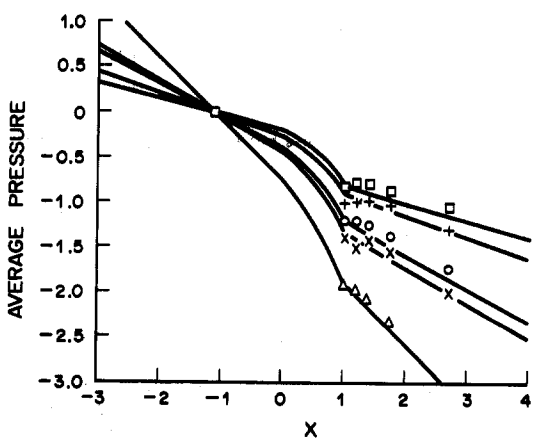

Figure 8. Liquid pressure vs the streamwise coordinate x for oil–water cases. +, $Q = 0.11$; □, $Q = 0.40$; △, $Q = 0.42$; ○, $Q = 0.57$; ×, $Q = 0.69$.

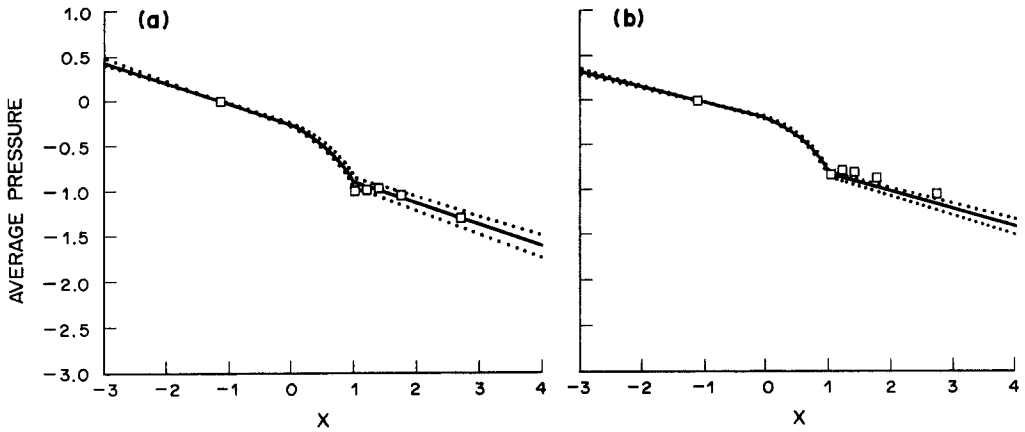

Figure 9. Liquid pressure vs the streamwise coordinate x for oil–water cases. Dashed lines are for $\pm 5\%$ deviations in the inlet flowrates. *Left*: $Q = 0.11$. *Right*: $Q = 0.41$.

agreement is good, both for air–water (figure 7) and oil–water (figure 8) cases. Some detail effects are present in the experiments which are not represented in the model. For example the "overshoot" in the pressure at $x = 1.0$ in each case is indicative of a small flow separation which occurs at the end of the conical contraction due to the sharp corner leading into the subsequent straight section of pipe. This would obviously not be seen in the one-dimensional model since the tappings are not actually modelled numerically but the pressure is obtained as a field throughout the pipe.

To illustrate quantitatively how good the agreement is in the pressure profile comparisons, the pressure profiles corresponding to a change of $\pm 5\%$ in the given flowrates at the inlet are plotted alongside the one calculated from the given flowrates and the experimental data points. Figure 9, for example, emphasizes two extreme cases for an oil–water mixture: the left graph is for the case where $Q = 0.11$, whereas the right graph is for $Q = 0.41$. In the second case, corresponding to

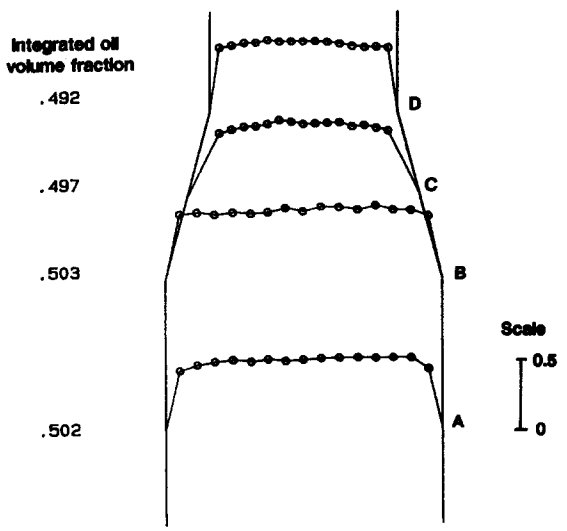

Figure 10. Local oil fraction distributions for oil–water flow with flowrate ratio $Q = 0.40$. The symbols represent measured data, with the lines merely joining the points for ease of reference. The plots are shown diagrammatically in their approximate axial locations relative to the contraction, with the integrated value of the volume fraction $(1/A)\int_{-D/2}^{D/2} \epsilon_b^{\downarrow} r\, dr$.

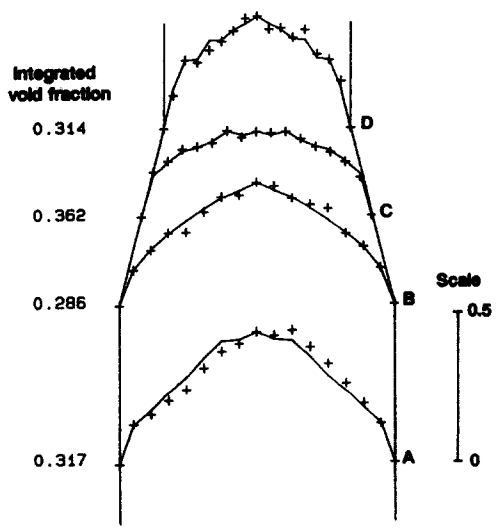

Figure 11. Local void fraction distributions for air–water flow with flowrate ratio $Q = 0.40$. The symbols represent the measured data, while the line joins points representing the average of the two values at that radius on either side of the centreline. The plots are shown diagrammatically in their approximate axial locations relative to the contraction, with the integrated value of the volume fraction $(1/A)\int_{-D/2}^{D/2} \epsilon_b^{\downarrow} r\, dr$.

a greater void fraction, the error is larger, consistent with the model limitation but even this magnitude of error is satisfactory for many design purposes.

It is interesting to consider the implication of this good agreement between experiment and theory bearing in mind the significant assumptions involved in the derivation. One major assumption is that the bubbly flow is made up of a uniform dispersion of uniformly sized spherical bubbles. From visual observations the oil–water flows appear to conform to this approximation, but the air–water flows show a wide range of bubble sizes and distributions. Figures 10 and 11 gave the local void fraction distributions for an oil–water flow and an air–water flow, respectively. It can be seen that the assumption of uniform distribution is quite reasonable for oil–water, but in error for air–water. Thus, the analysis seems robust to significant variations from the assumptions governing the derivation of the model, for reasons that are not readily apparent.

8. CONCLUSION

From the approach given by Kowe *et al.* (1988), we have derived a consistent and general set of equations to describe the motion of two phases (or components) in flow through a contraction. One phase is continuous, the other dispersed and the range of density ratios is wide. Given the density and flowrate of each component of the flow, the pressure, velocities and void fractions can be computed at any location alone the pipe. The single-phase limit as well as the homogeneous-flow limit are both contained within out set of equations. The full mathematical model requires only one fluid-dependent empirical input—the terminal rise velocity of a single bubble, U_t. This is in contrast to simpler models where extensive empirical calibrations are required. The use of the interstitial velocity and virtual-mass concepts removes the empiricism between the relative velocity, the void fraction and the terminal rise velocity.

Comparisons with experiments demonstrate that, although the model is one-dimensional and neglects local bubble–bubble interactions, it is nevertheless robust in dealing with vertical flow and a wide range of density ratios. U_t was obtained from standard correlations for the fluids used and was not artificially adjusted for these specific experiments. Both when $\rho = 1000$ or $\rho = 1.26$, the agreement between the mathematical predictions and the experiments was good in the vertical flow cases. The implication of this conclusion is that the model should perform well at any intermediate values of the density ratio.

Acknowledgement—The authors are grateful to Dr J. C. R. Hunt for his helpful conversations and suggestions.

REFERENCES

AUTON, T. R., HUNT, J. C. R. & PRUD'HOMME, M. 1988 The force exerted on a body in inviscid unsteady non-uniform rotational flows. *J. Fluid Mech.* **197**, 241–257.

BIESHEUVEL, A. & VAN WIJNGAARDEN, L. 1984 Two-phase flow equations for a dilute dispersion of gas bubbles in liquid. *Int. J. Multiphase Flow* **10**, 148.

BRUUN, H. H. & FARRAR, B. 1988 Hot-film probe studies of kerosene/water and gas/liquid flows. In *Experimental Heat Transfer, Fluid Mechanics and Thermodynamics* (Edited by SHAH, R. K., GANIC, E. N. & YANG, K. T.). Elsevier, New York.

CLIFT, R., GRACE, J. R. & WEBBER, M. E. 1978 *Bubbles, Drops and Particles*. Academic Press, London.

COOK, T. L. & HARLOW, F. H. 1984 Virtual mass in multiphase flow. *Int. J. Multiphase Flow* **10**, 691–696.

DARWIN, C. 1953 Note on hydrodynamics. *Proc. Camb. phil. Soc.* **49**, 342–354.

DREW, D. A. & LAHEY, R. T. 1979 Application of general constitutive principles to the derivation of multidimensional two-phase flow equations. *Int. J. Multiphase Flow* **5**, 243–264.

DREW, D. A. & LAHEY, R. T. 1987 The virtual mass and lift force on a sphere in rotating and straining inviscid flow. *Int. J. Multiphase Flow* **13**, 113–121.

GOVIER, G. W. & AZIZ, K. 1982 *The Flow of Complex Mixtures in Pipes.* Krieger, New York.
HARMATHY, T. Z. 1960 Velocity of large drops and bubbles in media of infinite or restricted extent. *AIChE Jl* **6,** 281–288.
KOWE, R., HUNT, J. C. R., HUNT, A., COUËT, B. & BRADBURY, L. J. S. 1988 The effects of bubbles on the volume fluxes and the pressure gradients in unsteady and non-uniform flow of liquids. *Int. J. Multiphase Flow* **14,** 587–606.
KUO, J. T. & WALLIS, G. B. 1988 Flow of bubbles through nozzles. *Int. J. Multiphase Flow* **14,** 547–564.
LAMB, H. 1945 *Hydrodynamics.* Dover, New York.
LEWIS, D. A. & DAVIDSON, J. F. 1985 Pressure drop for bubbly gas–liquid flow through orifice plates and nozzles. *Chem. Engng Des. Res.* **63,** 149–156.
NICOLAS, Y. & WITTERHOLT, E. J. 1972 Measurements of multiphase fluid flow. *Soc. Pet. Engrs* **4023.**
THOMAS, N. H., AUTON, T. R., SENE, K. & HUNT, J. C. R. 1983 Entrapment and transport of bubbles by transient large eddies in multiphase turbulent shear flow. Presented at the *Int. Conf. on the Physical Modelling of Multi-phase Flow*, Coventry, England, Paper E1, pp. 169–184.
WALLIS, G. B. 1969 *One-dimensional Two-phase Flow.* McGraw-Hill, New York.

APPENDIX

The liquid momentum equation is given by [36]:

$$\rho_l(2u_l-\epsilon_b u_b)\frac{du_l}{dx}+\rho_l u_l^2\frac{1}{A}\frac{dA}{dx}-\epsilon_b\rho_l C_m\left(u_b\frac{du_b}{dx}-u_l\frac{du_l}{dx}\right)+H$$
$$=-\epsilon_l\frac{dp_l}{dx}-\epsilon_l\rho_l g+\epsilon_b g|\Delta\rho|\frac{(u_b-u_l)|u_b-u_l|}{U_t^2},$$

with

$$H=\frac{\rho_l C_m}{10}\left\{4(u_b-u_l)^2\frac{\epsilon_b}{\epsilon_l}\frac{1}{A}\frac{dA}{dx}-\frac{d}{dx}\left[(u_b-u_l)^2\frac{\epsilon_b}{\epsilon_l}\right]\right\}.$$

To show that it reduces to Bernoulli's equation when $u_b=u_l$ (and trivially when $\epsilon_b=0$), the second term of the equation has to be rewritten using the continuity relation [13] and the fact that $u_l=u_L/\epsilon_l$ when there is no slip ($u_l=u_L$ for $\epsilon_b=0$) (see [8]):

$$\rho_l u_l^2\frac{1}{A}\frac{dA}{dx}=\rho_l u_l\frac{u_L}{\epsilon_l A}\frac{dA}{dx}$$
$$=-\rho_l\frac{u_l}{\epsilon_l}\frac{du_L}{dx}$$
$$=-\rho_l\frac{u_l}{\epsilon_l}\frac{d(\epsilon_l u_l)}{dx}$$
$$=-\rho_l\left(\frac{u_l^2}{\epsilon_l}\frac{d\epsilon_l}{dx}+u_l\frac{du_l}{dx}\right).$$

Following the definitions for the superficial velocities in section 2 and the equations of mass conservation in section 3.1, we have

$$\frac{d(Au_B+Au_L)}{dx}=0$$
$$=\frac{d[A\epsilon_b u_b+A(1-\epsilon_b)u_l]}{dx}$$
$$=\frac{d(Au_l)}{dx}$$

and

$$\frac{d(Au_L)}{dx} = 0$$

$$= \frac{d(A\epsilon_l u_l)}{dx}$$

$$= \epsilon_l \frac{d(Au_l)}{dx} + Au_l \frac{d\epsilon_l}{dx},$$

which therefore implies

$$\frac{d\epsilon_l}{dx} = 0$$

when $u_b = u_l$. Then, we have

$$\rho_l u_l^2 \frac{1}{A} \frac{dA}{dx} = -\rho_l u_l \frac{du_l}{dx}$$

when $u_b = u_l$, which, in turn, reduces the two first terms of [36] to $\epsilon_l \rho_l u_l \, du_l/dx$. Since the virtual-mass term, H and the drag term all vanish when there is no slip (as well as when $\epsilon_b = 0$), [36] becomes

$$-\rho_l u_l \frac{du_l}{dx} = \frac{dp_l}{dx} + \rho_l g.$$